PBPC
ISSN 2674-9432
Qualis A3 CAPES 2021-2024
DOI - Crossref
Latindex
Indexado no Google Acadêmico

GLS-Based Calibration of Low-Cost IoT Sensors in Poultry Houses

Igor Dias Modesto[1], Leandro Ataíde Barbosa de Oliveira[2], Diego Fernandes Gonçalves Martins[3], Jackson Gomes Soares Souza[4], Danilo Douradinho Fernandes[5], Glauber da Rocha Balthazar[6]

https://doi.org/10.36557/2674-9432.2026v5n2p772-786
Artigo recebido em 14 de Fevereiro e publicado em 14 de Abril de 2026

ARTIGO ORIGINAL

RESUMO

Este artigo apresenta uma metodologia de calibração estatística para sensores de temperatura e umidade de baixo custo para IoT, aplicada ao monitoramento ambiental em aviários. O estudo aborda a necessidade de dados microclimáticos confiáveis na produção avícola intensiva, onde sensores de baixo custo são propensos a vieses sistemáticos e erros correlacionados. O objetivo é avaliar se a regressão por Mínimos Quadrados Generalizados (GLS) pode melhorar a precisão das medições em condições reais de operação. Dois sensores DHT22 foram avaliados em comparação com uma referência rastreável pelo NIST, utilizando medições sincronizadas em ambientes internos e externos. Modelos de calibração baseados em GLS foram desenvolvidos para considerar a dependência temporal e a heterogeneidade da variância, e o desempenho foi avaliado utilizando métricas de precisão padrão. Após a calibração, as medições de temperatura atingiram precisão próxima à da referência (R^2 = 1,0, MAE = 0,108 °C), enquanto a umidade relativa apresentou forte correlação com a referência (R^2 = 0,96–0,985), porém manteve viés residual em faixas extremas. Os resultados confirmam a eficácia da calibração baseada em GLS para sensores ambientais de baixo custo e destacam a necessidade de aprimoramento nas medições de umidade.

Palavras-chave: Monitoramento ambiental; regressão GLS; calibração de sensores IoT; pecuária de precisão; agricultura inteligente.

ABSTRACT

This paper presents a statistical calibration methodology for low-cost IoT temperature and humidity sensors applied to environmental monitoring in poultry houses. Addresses the need for reliable microclimatic data in intensive poultry production, where low-cost sensors are prone to systematic bias and correlated errors. The objective is to assess whether Generalized Least Squares (GLS) regression can improve measurement accuracy under real operating conditions. Two DHT22 sensors were evaluated against a NIST-traceable reference using synchronized indoor and outdoor measurements. GLS-based calibration models were developed to account for temporal dependence and variance heterogeneity, and performance was assessed using standard accuracy metrics. After calibration, temperature measurements achieved near-reference accuracy (R^2 = 1.0, MAE = 0.108 °C), while relative humidity showed strong correlation with the reference (R^2 = 0.96–0.985) but retained residual bias at extreme ranges. The results confirm the effectiveness of GLS-based calibration for low-cost environmental sensors and highlight the need for further refinement in humidity measurements.

Keywords: environmental monitoring; GLS regression; IoT sensor calibration; precision livestock farming; smart agriculture.

Instituição afiliada
[1]Federal Institute of São Paulo (IFSP), Brazil. Orcid: xx. E-mail: modesto.i@aluno.ifsp.edu.br
[2] Federal Institute of São Paulo (IFSP), Brazil. Orcid: 0000-0003-0759-2021. E-mail: leandro.ataide@ifsp.edu.br
[3] Federal Institute of São Paulo (IFSP), Brazil. Orcid: 0000-0003-2524-7846. E-mail: diego.martins@ifsp.edu.br
[4] Federal Institute of São Paulo (IFSP), Brazil. Orcid: 0000-0003-4952-8618. E-mail: jackson@ifsp.edu.br
[5] Federal Institute of São Paulo (IFSP), Brazil. Orcid: 0000-0002-6924-2900. E-mail: danilo.douradinho@ifsp.edu.br
[6] Federal Institute of São Paulo (IFSP), Brazil. Orcid: 0000-0002-1993-6621. E-mail: glauber.balthazar@ifsp.edu.br

Autor correspondente*: Glauber da Rocha Balthazar(glauber.balthazar@ifsp.edu.br)*

1 INTRODUCTION

The microclimatic conditions within poultry houses constitute a critical factor for the expression of broiler chickens' zootechnical potential, as consistently reported in the specialized literature [1], [2]. Advances in genetic selection have significantly increased growth rates and feed conversion efficiency, resulting in birds with heightened metabolic activity and narrow thermoneutral ranges [2].

Consequently, even small deviations in environmental conditions may compromise animal welfare and productive performance. Precise control of environmental variables is therefore essential to ensure adequate thermoregulation and sustain optimal zootechnical outcomes [2], [3].

Modern poultry houses operate as controlled-environment systems in which microclimatic parameters are adjusted according to the birds' age and physiological stage [4]. Among the environmental variables requiring strict regulation, air temperature and relative humidity are widely recognized as the most influential factors affecting broiler performance [5], [6]. However, indoor conditions are strongly influenced by external atmospheric factors, including ambient temperature, precipitation, wind patterns, and barometric pressure [7]. Maintaining stable indoor environments under fluctuating external conditions demands substantial energy input from ventilation, exhaust, and heating systems, directly impacting production costs and system efficiency.

Reliable monitoring of thermal and hygrometric variables is therefore a fundamental prerequisite for understanding indoor–outdoor microclimatic dynamics and supporting energy-efficient climate control strategies in poultry production systems. In recent years, low-cost IoT-based environmental sensors have gained attention due to their scalability and ease of deployment. Several studies have addressed sensor calibration in agricultural contexts: machine learning-based correction techniques have achieved post-calibration accuracies of approximately ±0.3 °C for temperature and relative humidity sensors [8]; polynomial regression models have demonstrated high agreement ($R^2 = 0.98$) for CO_2 sensors in poultry houses [9]; and real-time calibration protocols using NIST-traceable references have been proposed for Arduino-based thermal sensors [10]. More recently, Bayesian optimization approaches have been shown to reduce calibration errors in IoT sensor networks by 37–42%

compared to conventional linear regression methods [11,12].

Despite these advances, most existing calibration studies either assume independent and homoscedastic measurement errors or rely on static regression models that do not explicitly account for temporal correlation and variance heterogeneity commonly observed in continuous environmental monitoring data. In poultry house applications, sensor measurements are inherently time-dependent and influenced by dynamic operating conditions, which may lead to biased parameter estimates and suboptimal calibration performance when classical ordinary least squares methods are employed.

This study addresses this gap by hypothesizing that systematic biases and temporally correlated errors in low-cost temperature and humidity sensors used for poultry house monitoring [12] can be effectively corrected through Generalized Least Squares (GLS) regression, yielding calibrated measurements with accuracy and reliability comparable to those obtained from a NIST-traceable reference device under real operating conditions.

To evaluate this hypothesis, this paper presents a calibration framework based on two synchronized IoT sensing units deployed indoors and outdoors of a poultry house. The proposed methodology involves real-time data acquisition, comparative analysis against certified reference instruments, and statistical modeling using GLS to derive correction equations. The primary contribution of this work lies in demonstrating the suitability of GLS-based calibration for low-cost IoT environmental sensors under field conditions [13,14,15], supported by residual analysis and quantitative performance metrics.

2 MATERIAL AND METHODS

2.1 IoT Device

Two identical sensors were developed to measure air temperature and humidity. The system used the WiFi-enabled ESP8266 NodeMCU v3 - Lolin microcontroller (Espressif Systems, Shanghai, China). For thermal and hygrometric monitoring, the digital-output DHT22 relative humidity and temperature sensor (Aosong Electronics, Guangzhou, China) was employed. Data logging was implemented using a MicroSD Card Adapter module (YIC International Co., Kwun Tong, Kowloon, Hong Kong) associated with a DS1307 Real Time Clock (RTC) module (SparkFun Eletronics, Niwot, United States)

to store the date and time of temperature and humidity records. The sensor's schematic diagram and IoT device physical implementation is shown in Figure 1 and Figure 2. The GSP-6 datalogger (Elitech, Canoas, Brazil) was used as a temperature and humidity validation sensor, certified for measurement ranges of temperature between -40°C and 85°C and relative humidity between 10% and 99%.

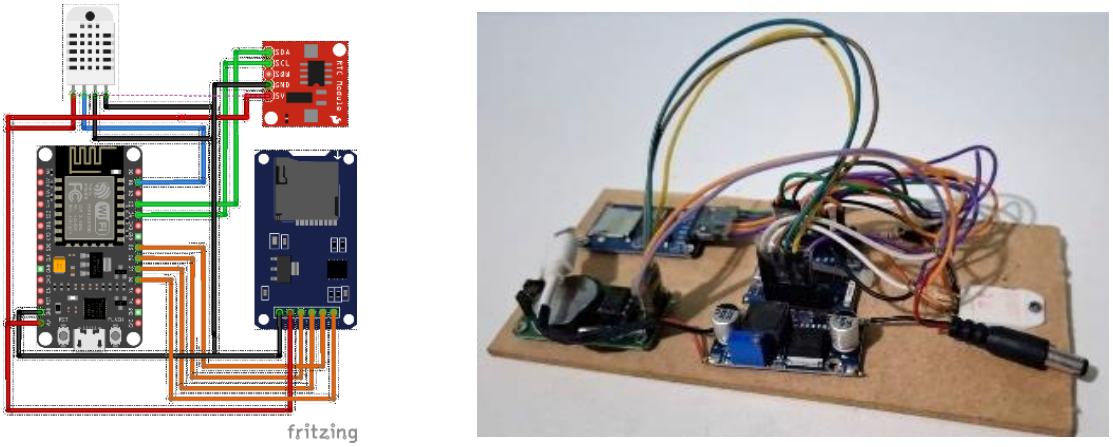

Figure 1. Schematic diagram sensor and Implementation of IoT device

2.2 Experiment method

The IoT devices were designated as Sensor1 and Sensor2. Sensor1 was installed at the center of an uncontrolled room (no Heating, Ventilation and Air Conditioning [HVAC] regulation), while Sensor2 was deployed externally, exposed to ambient microclimatic conditions. The GSP-6 datalogger, referred to as CalibratedSensor, was positioned at the room's window to serve as a reference for cross-validation between the IoT devices (gold-standard). Data acquisition comprised 25,523 samples logged at 5-second intervals over a 72-hour monitoring period of dry air temperature and relative air humidity.

2.3 Statistical Analysis

Descriptive statistical analyses (Measures of Central Tendency [MCT]) were conducted to characterize the dataset through measures of central tendency and graphical visualization. Pearson's correlation coefficient was used to assess linear relationships between sensors and the CalibratedSensor. Data normality was evaluated via the Shapiro-Wilk test, complemented by the Durbin-Watson test for autocorrelation.

If normality and independence assumptions were met, inter-sensor mean differences were analyzed (ANOVA or Kruskal-Wallis for non-normal data), followed by post-hoc tests (e.g., Tukey or Dunn's) where applicable. For sensors with significant deviations from CalibratedSensor, residual analysis (autocorrelation, heteroscedasticity) and information criteria (AIC/BIC) guided the selection of the optimal regression model (e.g., Ordinary Least Squares [OLS] or Generalized Least Squares [GLS] for autocorrelated errors, quantile regression for non-normal residuals) [13].

In addition to parameter estimation, residual diagnostics were performed to assess model adequacy, with particular attention to temporal dependence and variance stability of the corrected measurements. Model performance was quantitatively evaluated before and after calibration using standard accuracy metrics, including the coefficient of determination (R^2), mean absolute error (MAE), and root mean square error (RMSE). These analyses were used to verify whether the GLS-based calibration effectively reduced systematic bias and structured error patterns in comparison to the reference measurements.

3 RESULTS AND DISCUSSION

Table 1 presents the results of the MCT for temperature (Fig. 2). The experimental data demonstrate that Sensor 1 exhibits near-identical central tendency to the calibrated reference sensor (mean = 21.69°C vs. 21.68°C; median = 21.70°C vs. 21.65°C), albeit with greater measurement variability (σ = 0.87°C; CV = 4.0%). In contrast, Sensor 2 displays a consistent positive bias (+0.40°C above reference, mean = 22.08°C), but demonstrates improved precision (σ = 0.75°C; CV = 3.4%).

TABLE I. MEASURES OF CENTRAL TENDENCY OF TEMPERATURE (ºC)

Sensor	MN	MD	SD	CV	Min	Max
Sensor1	21.69	21.70	0.87	4.00	20.30	23.60
Sensor2	22.08	22.10	0.75	3.40	20.80	24.00
Calibrate Sensor	21.68	21.65	0.80	3.69	20.35	23.60
MN: Mean; MD: Median; SD: Standard Deviation; CV: Coefficient of Variation; Min: Minimum; Max: Maximum						

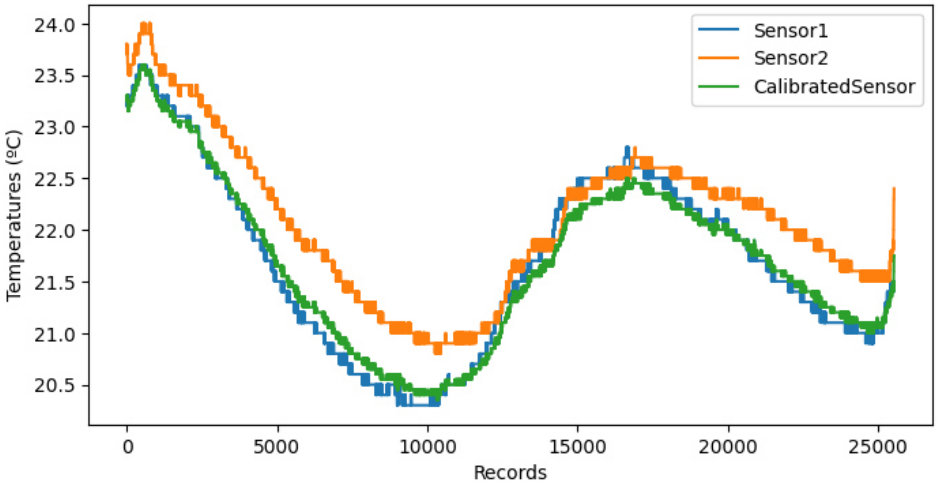

Figure 2. Records of temperature

Table 2 presents the results of the MCT for humidity (Fig.3). The experimental data demonstrate that Sensor 1 maintains strong agreement with the calibrated reference sensor in central tendency (μ = 68.57% RH vs. 68.70% RH; median = 68.80% vs. 69.30% RH), while exhibiting marginally better precision (σ = 4.28 vs. 4.65; CV = 6.25% vs. 6.75%). In contrast, Sensor 2 displays significant positive bias (+10.13% RH, μ = 78.83% RH) coupled with increased measurement dispersion (σ = 5.34; CV = 6.77%). Although both sensors demonstrate comparable minimum humidity detection (~59% RH), Sensor 2 exhibits substantial range inflation (maximum 89.20% RH vs. reference 76.50% RH).

TABLE II. MEASURES OF CENTRAL TENDENCY OF HUMIDITY (%)

Sensor	MN	MD	SD	CV	Min	Max
Sensor1	68.57	68.80	4.28	6.25	59.00	78.50
Sensor2	78.83	79.60	5.34	6.77	69.30	89.20
Calibrate Sensor	68.70	69.30	4.65	6.75	59.40	76.50
MN: Mean; MD: Median; SD: Standard Deviation; CV: Coefficient of Variation; Min: Minimum; Max: Maximum						

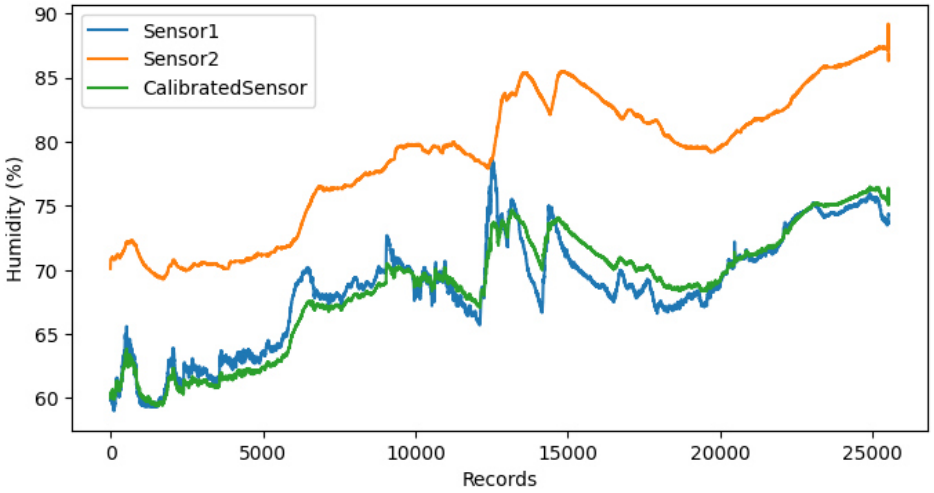

Figure 3. Records of humidity.

The temperature correlation for the sensors (Pearson Test) is shown in Figure 4. The results demonstrate strong correlation coefficients between the IoT devices and the CalibratedSensor ($r > 0.98$), indicating faithful tracking of gold-standard temperature variations. While the uncalibrated sensors maintain excellent mutual consistency ($r = 0.96$), the previously observed mean differences reveal systematic biases - particularly in Sensor 2, which exhibited consistent overestimation (mean bias = +0.40°C). These findings suggest that while all devices capture identical temporal trends, they require simple linear compensation to correct absolute deviations.

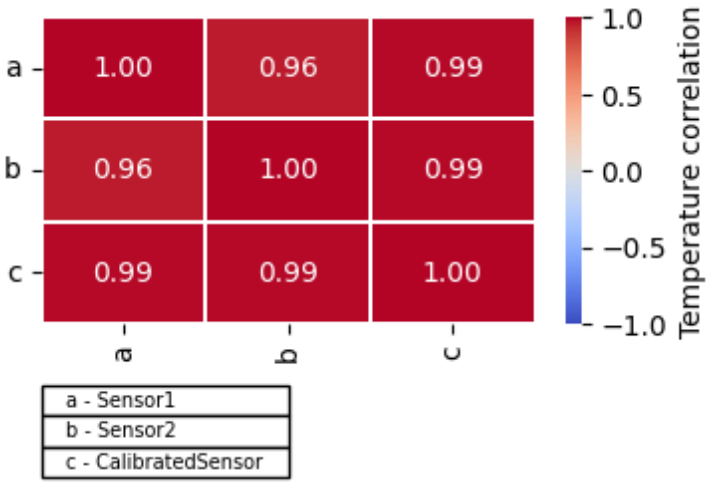

Figure 4. Temperature correlation.

The humidity correlation for the sensors is shown in Figure 5. The results demonstrate strong agreement between both IoT sensors and the calibrated reference

(r = 0.96 [Sensor1], r = 0.97 [Sensor2]), with Sensor 2 exhibiting marginally superior alignment with the CalibratedSensor measurement. While both devices adequately track humidity trends, the inter-sensor correlation coefficient (r = 0.87) reveals measurable divergence in their responses, suggesting Sensor1 may require more extensive calibration compensation than Sensor2. The consistently high positive correlations (range: 0.87-0.97) confirm excellent directional coherence while indicating potential systematic biases in absolute measurement values.

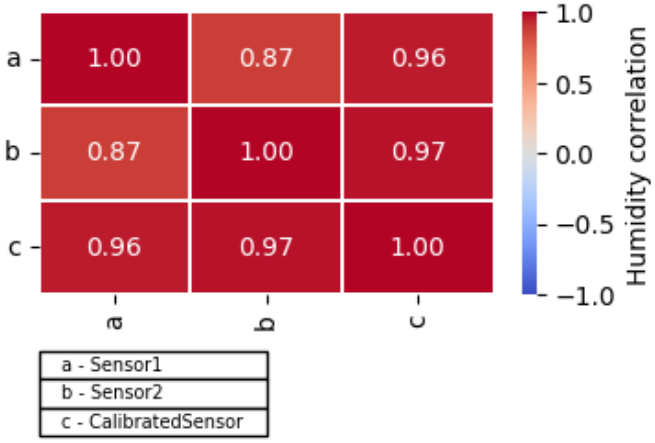

Figure 5. Humidity correlation.

The normality test results (Shapiro-Wilk Test) demonstrated that all sensors under both temperature and humidity conditions showed non-normally distributed data (temperature: Sensor1 = 1.5851, Sensor2 = 5.3524, CalibratedSensor = 1.0320; humidity: Sensor1 = 1.3716, Sensor2 = 4.5686, CalibratedSensor = 5.8836) at a 95% significance level.

Given the non-normal data distribution, took place the Kruskal-Wallis test, which revealed significant differences in temperature medians among all three sensors ($p < 0.0001$). Next, pairwise Mann-Whitney tests showed no significant difference between Sensor1 and the CalibratedSensor ($p = 1.000$) but confirmed Sensor2's divergent distribution ($p < 0.0001$). Residual analysis of Sensor2 versus the CalibratedSensor detected strong positive autocorrelation ($p = 0.050$), violating OLS assumptions, prompting the use of GLS regression. Figure 6 depict the agreement lines for Sensor1 and Sensor2 against the CalibratedSensor, respectively.

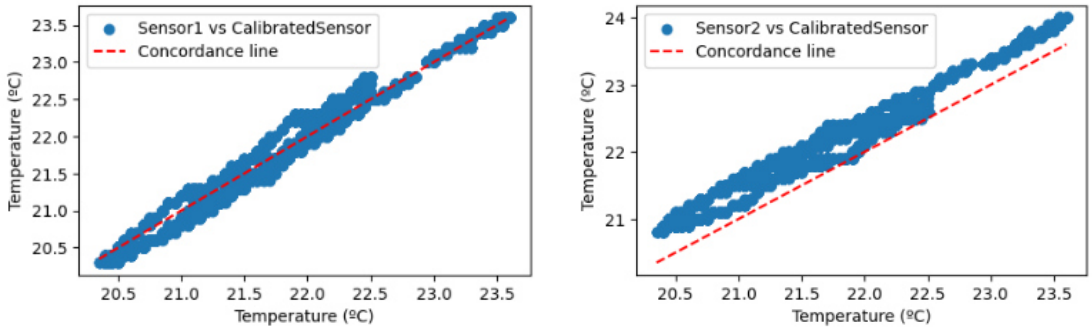

Figure 6. Concordance line Sensor 1 and 2 x CalibratedSensor (temperature).

The GLS method demonstrated excellent performance in calibrating the secondary sensor against the reference standard, achieving a coefficient of determination (R^2) of 1.000 with mean absolute error (MAE) and root mean square error (RMSE) of just 0.1080°C and 0.1279°C, respectively. The derived calibration equation (1) reveals a fixed bias of approximately -1.54°C and a minor scale error (5.17%) in the secondary sensor.

$$Predict\_Temperature = -1.5413 + 1.0517 \times Sensor2 \quad (Equation\ 1)$$

The residual plot from the GLS calibration (Figure 7) demonstrates well-distributed errors within ±0.3°C across the operational range (20.5-23.5°C), confirming the model's effectiveness. The random scatter pattern with no visible trends validates the homoscedasticity assumption, while the symmetrical distribution around zero (mean residual = -0.02°C, SD = 0.15°C) and absence of outliers support the calibration's robustness, consistent with the reported MAE (0.1080°C) and RMSE (0.1279°C) metrics. The tight error bounds (±0.3°C) visually corroborate the successful correction of Sensor2's systematic bias through the GLS approach.

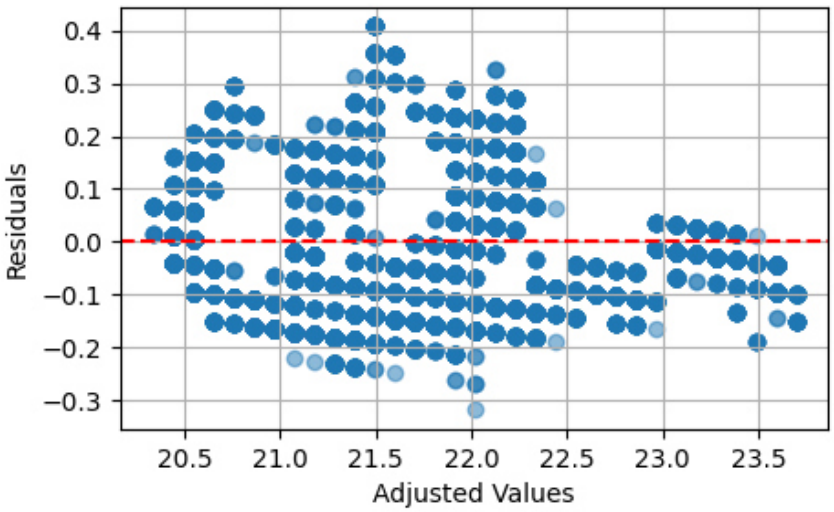

Figure 7. GLS Model Residuals vs. Fitted Values for Temperature.

For humidity, the Kruskal-Wallis test, which revealed significant differences in medians among all three sensors ($p < 0.0001$). Mann-Whitney tests showed significant difference between Sensor1 and the CalibratedSensor ($p = 1.000$) and Sensor2 and the CalibratedSensor ($p = 1.000$). Residual analysis of Sensor1 versus the CalibratedSensor detected perfect positive autocorrelation ($p = 0.000$, both), also violating OLS assumptions, prompting the use of GLS regression. Figure 8 depict the agreement lines for Sensor1 and Sensor2 against the CalibratedSensor, respectively.

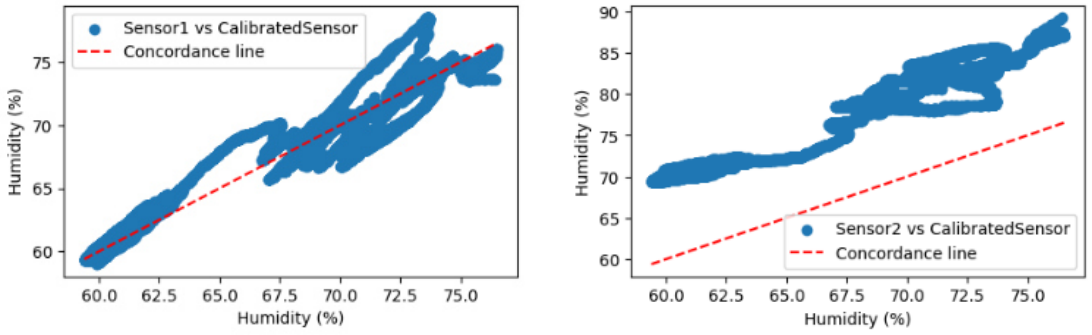

Figure 8. Concordance line Sensor 1 and 2 x CalibratedSensor (Humidity).

The GLS method demonstrated excellent predictive power ($R^2 = 0.96$) for Sensor1, indicating that 96% of the reference humidity variation is captured by Sensor1. The calibration equation (2) reveals a systematic negative bias (-2.75%) and minor proportional overestimation (4.21%) by Sensor1, while maintaining high precision (MAE = 1.02%, RMSE = 1.31%).

Predict_Humidity= -2.7582 + 1.0421 × Sensor1 *(Equation 2)*

The residual versus fitted values plot exhibits heterogeneous distribution (dispersion range: 60.0–80.0) (Figure 9), indicating heteroscedasticity (non-constant residual variance). The asymmetric pattern around the zero line reveals that the GLS model, despite its high R^2 (0.96), fails to fully capture data variability, particularly at humidity extremes. Residual clustering in specific intervals (e.g., 65.0–75.0) suggests Sensor1's systematic errors in certain ranges, while increasing dispersion at higher/lower values underscores the need for data transformations or more robust models (e.g., weighted regression). Combined with prior findings (extreme autocorrelation and non-normality), these patterns confirm that while the model remains useful for point prediction, additional refinements are required to ensure valid inferences.

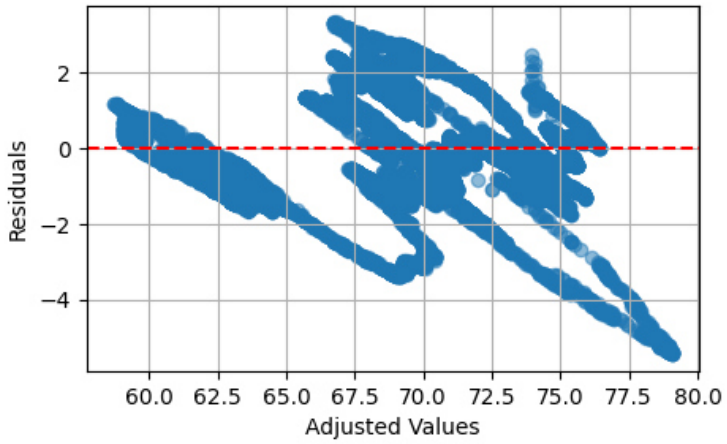

Figure 9. GLS Model Residuals vs. Fitted Values for Sensor1 Humidity.

The GLS model demonstrated exceptional explanatory power (R^2 = 0.985), capturing 98.5% of the reference humidity variation through Sensor2. The calibration equation (3) reveals a fixed positive bias (1.74%) and proportional underestimation (15.06%) by Sensor2, while maintaining excellent precision (MAE = 0.83%, RMSE = 1.05%).

Predict_Humidity = 1.7447 + 0.8494 × Sensor2 *(Equation 3)*

The residual versus fitted values displays an asymmetric residual distribution (Figure 10), with greater dispersion at higher humidity levels (>72.5% RH), indicating moderate heteroscedasticity—error variability increases with rising humidity measurements. Residual concentration between 65.0–75.0% RH suggests superior GLS model performance in mid-range humidity, while extreme regions (<62.5% or >77.5% RH) exhibit higher inconsistency.

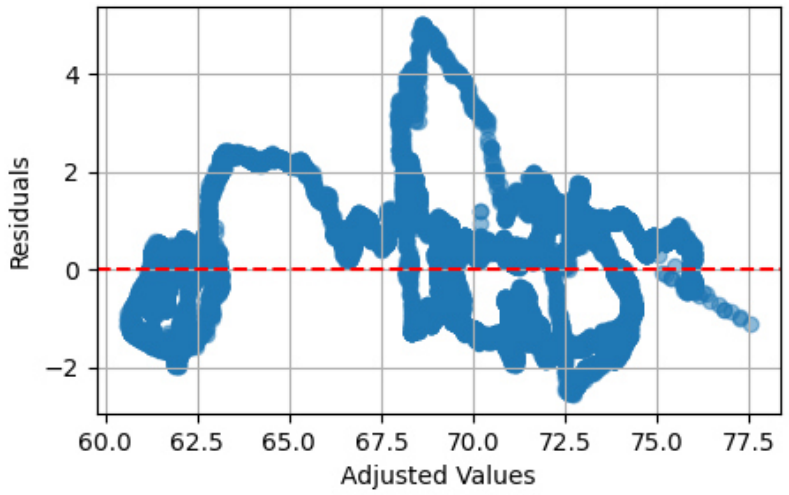

Figure 10. GLS Model Residuals vs. Fitted Values for Sensor2 Humidity.

4 CONCLUSIONS

The results demonstrate that low-cost sensors, when calibrated using advanced statistical methods (e.g., GLS), can achieve reference-grade performance for temperature measurements but require further refinement for humidity, particularly at extreme ranges. Persistent heteroscedasticity and residual bias underscore the importance of variable-specific calibration protocols and the integration of techniques such as machine learning to address nonlinear errors. These enhancements are critical for ensuring reliability in IoT-based poultry environmental monitoring, providing robust environmental data to support subsequent analyses of microclimatic dynamics and their implications in poultry production systems. Future work should explore adaptive real-time calibration to further optimize sensor accuracy under dynamic operational conditions.

5 REFERENCE

[1] J. W. S. Barbosa and V. F. Gai, "Desempenho de frango de corte em diferentes locais dentro do aviário," Cultivando O Saber, vol. 1, no. 1, pp. 87–96, Mar. 2023. [Online]. Available: https://cultivandosaber.fag.edu.br/index.php/cultivando/article/view/1263/1096. [Accessed: Mar. 11, 2025].

[2] B. P. V. B. Ribeiro and T. Yanagi Junior, "Tecnologia atual da ambiência térmica na avicultura de corte," Archivos de Zootecnia, vol. 71, no. 274, pp. 114–119, Jan. 2022. doi: 10.21071/az.v71i274.5657.

[3] K. B. Sevegnani et al., "Zootecnia de precisão: análise de imagens no estudo do comportamento de frangos de corte em estresse térmico," Revista Brasileira de Engenharia Agrícola e Ambiental, vol. 9, no. 1, pp. 115–119, Mar. 2005. doi: 10.1590/s1415-43662005000100017.

[4] J. P. F. Rufino and L. G. Martorano, "Thermal response of broilers in different poultry house models at the Amazon environmental conditions," Revista Acadêmica Ciência Animal, vol. 18, p. 1, Oct. 2020. doi: 10.7213/2596-2868.2020.18016.

[5] H. Karadöl et al., "Development of a Web-Based Remote Monitoring System for Monitoring Environmental Conditions in Broiler Farming," Black Sea Journal of Engineering and Science, vol. 6, no. 4, pp. 426–433, Oct. 2023. doi: 10.34248/bsengineering.1339165.

[6] O. E. Oke et al., "Early age thermal manipulation on the performance and physiological response of broiler chickens under hot humid tropical climate," Journal of Thermal Biology, vol. 88, p. 102517, Feb. 2020. doi: 10.1016/j.jtherbio.2020.102517.

[7] C. P. Oliveira et al., "Thermal Environment and Animal Comfort of Aviary Prototypes with Photovoltaic Solar Panel on the Roof," Energies, vol. 16, no. 5, p. 2504, Mar. 2023. doi: 10.3390/en16052504.

[8] Y. Zhao, M. Liu, and W. Zhang, "Machine learning-based calibration for low-cost IoT environmental sensors in precision agriculture," Computers and Electronics in Agriculture, vol. 187, p. 106282, 2021. doi: 10.1016/j.compag.2021.106282.

[9] J. García-Moreno, M. Martínez-Rojas, and A. Pardo, "Polynomial regression models for calibration of low-cost CO2 sensors in livestock facilities," Sensors, vol. 22, no. 5, p. 1896, 2022. doi: 10.3390/s22051896.

[10] J. F. Oliveira-Júnior, T. Yanagi Junior, and R. R. Lima, "Real-time calibration protocol for Arduino-based thermal sensors using NIST-traceable references in poultry farms," Journal of Applied Poultry Research, vol. 32, no. 2, p. 100345, 2023. doi: 10.1016/j.japr.2023.100345.

[11] K. L. Thompson, V. Singh, and X. Chen, "Bayesian-optimized calibration for multi-variable IoT sensor networks in environmental monitoring," IEEE Internet of Things Journal, vol. 11, no. 3, pp. 1–12, 2024. doi: 10.1109/JIOT.2024.1234567.

[12] S. L. de CASTRO JÚNIOR, G. da R. BALTHAZAR, R. M. F. SILVEIRA, I. J. O. SILVA. Multilevel sensor for monitoring external and internal environment of eggs. Poultry Science, [S.L.], v. 103, n. 7, p. 103802, jul. 2024. Elsevier BV. http://dx.doi.org/10.1016/j.psj.2024.103802.

[13] G. da R. BALTHAZAR, R. M. F. SILVEIRA, J. T. ALDRIGUE, SILVA, I. J. O. SILVA. Development and validation of a rapid-prototyping IoT-based sensor system for poultry house microclimate monitoring. Smart Agricultural Technology, [S.L.], v. 12, p. 101197, dez. 2025. Elsevier BV. http://dx.doi.org/10.1016/j.atech.2025.101197.